INTERNATIONAL JOURNAL FOR NUMERICAL METHODS IN FLUIDS
*Int. J. Numer. Meth. Fluids* **28**: 1159–1181 (1998)

# TRANSIENT FINITE ELEMENT ANALYSIS OF GENERALIZED NEWTONIAN COEXTRUSION FLOWS IN COMPLEX GEOMETRIES

ALBERTO J. RINCÓN[1], ANDREW N. HRYMAK* AND JOHN VLACHOPOULOS
*CAPPA-D, Department of Chemical Engineering, McMaster University, Hamilton, Ontario L8S 4L7, Canada*

## SUMMARY

A two-dimensional transient finite element model capable of simulating problems related to two-layer polymer flows has been developed. This technique represents an effective tool which can be used to study the possibility of the onset of interfacial instability in coextrusion flows, considering melt rheology as well as the fluid–geometry interaction. A code has been developed to solve the transient problem of the flow of bi-component systems of Newtonian and generalized Newtonian fluids through parallel plates and complex geometries, such as: 2:1 abrupt expansion, 2:1 (30°) expansion, 4:1 abrupt contraction and 4:1 tapered (30°) contraction. Solutions are compared with experimental data from the literature and results provided by linear stability analysis (LSA) for the case of parallel plate flows. Numerical results are in agreement with LSA results for the parallel plate geometry cases studied. The expansion geometries tend to stabilize flows in the parallel plate section downstream of the expansion. Contractions may give rise to break-up of the interface depending on the flow conditions. © 1998 John Wiley & Sons, Ltd.

KEY WORDS: coextrusion; interfacial instability; transient simulation

## 1. INTRODUCTION

Coextrusion is the simultaneous extrusion from a single die of two or more homogeneous melts which form a lamellar structure. Resins are in separate extruders and a single extruder can supply more than one layer of the same resin. In recent years, coextrusion has gained importance because it is an economical and effective method to obtain plastic products that meet specific market requirements.

Two types of problems exist in the coextrusion process: interfacial flow instability and non-uniform layer-thickness distribution. Non-uniform layer distribution refers to the change in thickness of the distribution of the layers across the width of the sheet [1]. Interfacial flow instability manifests itself in three different forms: zig-zag, scattering and wave instabilities [2–6].

The wave instability is seen as a train of parabolas following the flow direction spanning the width of the extruded sheet [2]; currently, the reasons for its onset are poorly understood. Recent experimental work [2] suggests that the geometry of the die plays a key role in the onset of this instability.

* Correspondence to: CAPPA-D, Department of Chemical Engineering, McMaster University, Hamilton, Ontario, Canada L8S 4L7.
[1] Research performed while on leave from: 'Investigación y Desarrollo C.A.' (INDESCA), Complejo Petroquimico el Tablazo, Edo. Zulia, Venezuela.

CCC 0271–2091/98/181159–23$17.50

*Received 3 January 1997*
*Revised 13 January 1998*

Wilson and Khomami [7–10] examined interfacial instabilities in two-layer coextrusion flows by introducing temporally regular disturbances with a controllable amplitude and frequency in the transfer line of one of the extruders. The perturbation was of the form of a pressure pulse ($P = A \sin \omega t$) with the amplitude, $A$, between 0.5 and 5% of the average channel pressure (400–500 psi), and $\omega$ identical to the screw rotation frequency, with a typical value of 20 Hz. If the interfacial wave had a negative growth rate, the flow was considered to be stable. A positive growth rate would indicate the presence of an unstable flow. Typical values of the growth rate varied between 0.001 cm(amplitude)/cm(die length) and 0.005 cm/cm.

A recent study by Hyun and Spalding [11] indicates that fluctuations in pressure at the discharge of an extruder can cause instantaneous changes in the die output rate, generating fluctuations in the dimensions of the product (transient behaviour). However, the study shows that periodic oscillations caused by screw rotation are not related to the lower frequency flow surging. Unsteady state behaviour, such as inconsistent solids conveying and solid bed break-up [12], can impose low frequency disturbances onto the higher frequency screw rotation perturbation.

A number of authors have analyzed the problem of interfacial instability by using linear stability analysis (LSA) to determine which flow rate and viscosity ratio values characterize stable or unstable flows. LSA provides valuable information in the form of stability diagrams for specific types of coextrusion flows in which stable and unstable zones are identified. To study the instability of an interface, LSA considers two-dimensional infinitesimal disturbances of the steady state solution of the velocity, pressure, and extra stress tensor. The analysis assumes that all perturbation quantities have an exponential time and periodic spatial dependence of the form

$$q(x, y, \theta) = \bar{q}(y)\, \mathrm{e}^{i\alpha(x - c\theta)}, \tag{1}$$

where $q$ represents an arbitrary perturbation variable, $q(y)$ is the amplitude of the disturbance, $\alpha$ is a real positive number inversely proportional to the wavelength, $x$ is the flow direction, $\theta$ is the dimensionless time, and $c$ is a complex number. Stability is governed by the sign of the imaginary part of $c$: if it is positive, the amplitude of the disturbance increases with time and the flow is unstable; if it is negative, the flow is stable. The governing equations are linearized with respect to perturbation quantities and the resulting eigenvalue problem solved with the complex wave speed $c$ as the eigenvalue for which the neutral stability lines are determined.

Table I summarizes relevant papers using linear stability analysis. The major limitation of the linear stability methodology is that only relatively simple geometries can be modelled. Complex geometries, such as those in industrial coextrusion dies, are not amenable to standard linear stability analysis techniques. This limitation can be overcome with the use of numerical methods which allow the study of die design, processing conditions and rheology in coextrusion. The nature of stratified flow makes coextrusion simulation a non-linear problem. The interface (internal free surface) location is not known *a priori* and must be included in the calculation. Additional sources of non-linearity derive from the non-linear properties of the polymer melts and the complexity of the die geometries.

Computer simulation of two-layer flat steady state coextrusion has been carried out in 2D [26,27] and 3D geometries [28]. The problem of the discontinuity of pressure and material properties across the interface has been tackled using finite elements following two approaches: approximate the pressure in a continuous form in each of the two components and introduce double nodes at the interface [26,27,29] or approximate the pressure in a discontinuous form [30,31]. The finite element simulation of the flow of stratified fluids in steady state for complex

 

geometries has been the subject of a number of works [30–33]. The geometries studied have included 4:1 abrupt and tapered expansions and contractions.

The literature reports many studies dealing with unsteady free surface flow problems involving a liquid–air interface. Their main features have been the time dependency of the flow domain and the representation of the free surface and its boundary conditions. A mixed Eulerian–Lagrangian formulation [34] interpolates the unknown flow field by finite element basis functions on a continuously deforming grid. The displacement of the free surface is unknown *a priori* and is determined with the unknown fields and, at each time step, the grid is deformed to follow the movement of the free surface [35–39].

Anturkar [40] used a streamlined transient Galerkin finite element formulation to solve the problem of a bi-component flow system of Newtonian and viscoelastic fluids respectively, between parallel plates. A wavy pattern was obtained for the interfacial shape but with no visible growth or decay in amplitude.

In this work, a study of the interfacial stability of different bi-component Newtonian and generalized Newtonian flow systems is presented. The results are compared with experimental evidence concerning the existence of low frequency disturbances entering the die from the extruder and its effect on the final coextrudate. A transient finite element code has been devised to solve a variety of bi-component flow systems in which one of the inlet volumetric flow rates is periodically perturbed in time. By analyzing the transient response of the interface between the two fluids to the external perturbation, the stability of the flow systems is investigated.

In terms of the nature of the problems solved, the work can be divided into three parts: the bi-component flow problem for the case of a straight channel with a comparison of results against LSA theory; bi-component flows through complex geometries; and calculations for the case presented in the experimental work of Wilson and Khomami [7,10] on the stability of high density polyethylene (HDPE)/ polypropylene (PP) coextrusion flow systems through a flat die [7].

Table I. Linear stability analysis, results applicable to the coextrusion problem

| Authors | Fluid | Geometry | Parameters studied |
|---|---|---|---|
| Yih [13] | Newtonian | Plane Couette<br>Plane Poiseuille | Viscosity ratio |
| Hickox [14] | Newtonian | Plane Couette | Viscosity ratio |
| Li [15] | Oldroyd fluid | Plane Couette | Viscosity ratio |
| Khan and Han [16] | Colleman-Noll second order fluid | Rectangular duct | Viscosity ratio |
| Chen [17] | Upper convected Maxwell fluid | Plane Couette | Elasticity, viscosity and density ratios |
| Hooper and Boyd [18] | Newtonian | Unbounded Couette | Surface tension, density ratio |
| Joseph, Renardy and Renardy [19] | Newtonian | Poiseuille core-annular flow in tube | Viscosity ratio |
| Waters [20] | Power law | Plane Couette | Shear thinning viscosity (power law parameters) |
| Khomami [21,22] | Power law | Plane Poiseuille | Shear thinning viscosity (power law parameters) |
| Su and Khomami [23–25] | Oldroyd-B | Plane Poiseuille | Elasticity, viscosity and density ratios |

 

## 2. GOVERNING EQUATIONS

The flow of molten polymers inside the die has been modelled assuming creeping, isothermal and incompressible flow with no body forces.

The governing equations expressing conservation of momentum and mass are

$$\rho \frac{DV}{Dt} = \nabla \cdot \tau - \nabla P, \tag{2}$$

$$\nabla \cdot V = 0. \tag{3}$$

The material derivative of the velocity in Equation (2) is

$$\rho \frac{DV}{Dt} = \rho \frac{\partial V}{\partial t} + \rho V \cdot \nabla V. \tag{4}$$

Nodes move depending on the movement of the interface along a fixed line in space (spine). This corresponds to a mixed Eulerian–Lagrangian formulation. However, the time derivative of Equation (4) is a Eulerian time derivative, i.e. the nodal velocity field is defined for nodes fixed in space. Therefore, the time derivative $(\partial/\partial t)$ is transformed to a time derivative which follows the moving nodes along the spines $(\delta/\delta t)$.

The relationship between $\delta/\delta t$ and $\partial/\partial t$ is

$$\frac{\delta}{\delta t} = \frac{\partial}{\partial t} + \frac{\partial X}{\partial t} \cdot \nabla = \frac{\partial}{\partial t} + \frac{\delta h}{\delta t} \frac{\partial X}{\partial h} \cdot \nabla, \tag{5}$$

where $X = X(h, \xi, \eta)$ is the vector of co-ordinates of a moving nodal point and $h$ is the interface position. The term $\partial V/\partial t$ (obtained when the velocity vector $V$ is substituted into Equation (5) is substituted into the momentum equation (4), and the resulting equation is

$$\rho\left(\frac{\delta V}{\delta t} - \frac{\delta h}{\delta t} \frac{\partial X}{\partial h} \cdot \nabla V + V \cdot \nabla V\right) = \nabla \cdot \tau - \nabla P. \tag{6}$$

The flows considered are two-dimensional, with the velocity expressed as $V = ui + vj$. $\tau$ is the extra stress tensor and $P$ is the pressure. A generalized Newtonian constitutive equation [41] is used to model the stress–strain relation:

$$\tau_{ij} = \eta\left(\frac{\partial V_i}{\partial X_j} + \frac{\partial V_j}{\partial X_i}\right). \tag{7}$$

The viscosity dependence on shear rate can be modelled either as Newtonian ($\eta = \text{constant}$) or fit to a Carreau model, which is of the form

$$\eta(\dot{\gamma}) = (\eta_0 - \eta_\infty)[1 + (\lambda\dot{\gamma})^a]^{(n-1)/a}, \tag{8}$$

where $\eta_0$, $\eta_\infty$, $\lambda$, $a$ and $n$ are material properties, and

$$\dot{\gamma} = \sqrt{\frac{1}{2} II_\gamma}. \tag{9}$$

Figure 1 shows a schematic of the different geometrical domains included in this work: a straight channel, an abrupt and a tapered (30°) 2:1 expansion, and an abrupt and a tapered (30°) 4:1 contraction. Figure 1(a), containing reference labels, will be referred to below to specify the boundary conditions. Similar boundary conditions are applied to the rest of the different domains in Figure 1(b–e).

 

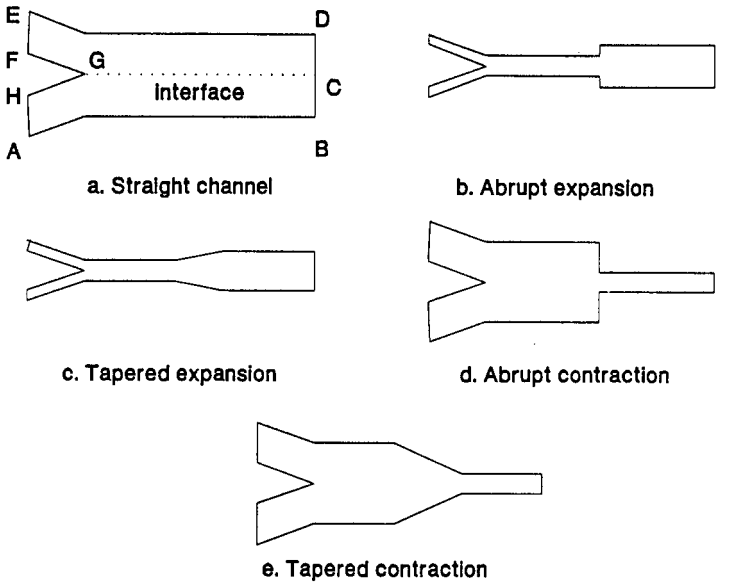


Figure 1. Schematic of different geometrical domains.

The boundary conditions assume fully developed flow at the die inlet for each of the two channels. A sinusoidal perturbation in time ($t$) of the fully developed velocity profile of fluid 1 entering feed channel 1 (lines HA in Figure 1(a)) is imposed. The fully developed velocity profile of fluid 2 entering channel 2 (line EF in Figure 1(a)) remains constant in time:

$$\text{On HA } (n \cdot V)_1 = f_1(x, y, t), \tag{10}$$

$$\text{On EF } (n \cdot V)_2 = f_2(x, y). \tag{11}$$

The no-slip boundary condition is applied at solid boundaries (see Figure 1):

$$\text{On AB, DE, FGH, } V = 0. \tag{12}$$

At the interface GC, interfacial tension is neglected since viscous forces are extremely high compared with interfacial tension [1], and the boundary conditions are expressed as

– Equilibrium of forces:

$$n \cdot \sigma_1 = n \cdot \sigma_2, \qquad t \cdot \sigma_1 = t \cdot \sigma_2, \qquad \sigma_k = -P_k \cdot I + \tau_k, \quad k = 1, 2, \tag{13}$$

– Continuity of tangential velocities and vanishing velocity normal to the interface:

$$t \cdot \left( V - \frac{\partial X}{\partial t} \right)_1 = t \cdot \left( V - \frac{\partial X}{\partial t} \right)_2. \tag{14}$$

At the exit, line BCD, zero traction and zero cross flows ($v = 0$) are imposed at each time step. However, the interface is allowed to move at the exit plane ($\delta h / \delta t \neq 0$) in order to satisfy continuity.

 

## 3. FINITE ELEMENT METHOD

The type of elements used in this work are quadrilateral nine-node quadratic Lagrangian elements for the velocity field $V$ and quadrilateral four-node bilinear elements for the pressure field $P$. Velocity, nodal co-ordinates and pressure are interpolated within an element by

$$V_i^{(e)}(t) = \sum_i N^i(\xi, \eta) V_i, \tag{15}$$

$$X_i^{(e)}(t) = \sum_i N^i(\xi, \eta) V_i, \tag{16}$$

$$P^{(e)}(t) = \sum_i N_P^i(\xi, \eta) P_i. \tag{17}$$

The dependence of the nodal locations $X(h)_i$ on the position of the interface is given by Equation (16).

The interface is described using the spine technique of Kistler and Scriven [37]. A spine is a line that is defined by the location of a static base point $x_{\mathrm{B}}^k$, a static top point $x_{\mathrm{T}}^k$ and its inclination $e^k$, as in Figure 2 for the linear case. The interface is defined by its distance from the base points $x_i^k$.

Elements are deformed corresponding to the deformation of the interface, by positioning the nodes at fixed proportions, $w^i$, along a spine aligned in the gap direction so that they move in proportion to the interface. The location of the node $i(k, j)$ on the $k$th spine is:

For nodes located under or at the interface:

$$x^i = x_{\mathrm{B}}^k + w^j h^k (x_{\mathrm{T}}^k - x_{\mathrm{B}}^k). \tag{18}$$

For nodes above the interface:

$$x^i = x_{\mathrm{B}}^k + (x_{\mathrm{T}}^k - x_{\mathrm{B}}^k)(h^k + w^j(1 - h^k)). \tag{19}$$

In Equations (18) and (19), the dimensionless interface position $h^k$ is given by

$$h^k = \frac{x_i^k - x_{\mathrm{B}}^k}{x_{\mathrm{T}}^k - x_{\mathrm{B}}^k}. \tag{20}$$

At the element level, the interface is described by the finite element representation:

$$x_i = \sum_{j=1}^{ni} x_i^j N^j \quad (\xi, \eta = 1), \tag{21}$$

where $ni$ is the number of nodes on the interface.

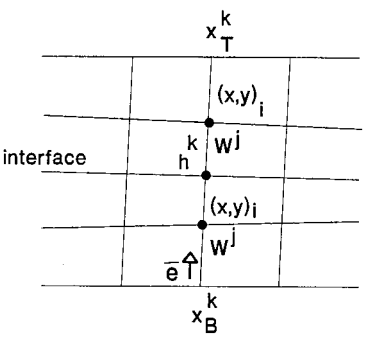


Figure 2. Moving node position definition.

 

The dynamic simulation uses a steady state solution of Equations (2), (3), (7) or (8), and (10)–(14) as the initial state corresponding to time step 0. A sinusoidal perturbation is imposed on the fully developed velocity profile at the entrance of the feeding channel corresponding to fluid 1 (lower fluid) and the evolution in time of the interface observed.

In order to determine the stability of a given flow system, the different transient vertical positions of interfacial points at fixed locations along the die length are collected, and their cyclic behaviour monitored. If the maximum amplitude of the resulting wave decreases in the flow direction, the flow is said to be stable. In the contrary case, it would be considered unstable [7].

The time dependent inlet velocity profile is of the form

$$V_1(x, y, t) = V_1(x, y) + A \sin(\omega t), \tag{22}$$

where $A$ is the amplitude of the perturbation and $\omega$ is its frequency in rad $s^{-1}$.

An independent variable used in the numerical experiments is the dimensionless wavenumber $\alpha$, defined as

$$\alpha = \frac{\omega d}{V_{\text{int f}}}, \tag{23}$$

where $d$ is the steady state thickness of the more viscous layer (lower layer) and $V_{\text{int f}}$ is the steady state velocity of the interface at the exit of the die.

A Galerkin method is used to reduce the governing differential equations (Equations (2) and (3)) and the kinematic boundary condition (14) to a first-order system of differential equations, written as

$$[C]\{\dot{U}\} + [K]\{U\} = \{F\}, \qquad \{U(t_0)\} = \{U_0\}, \tag{24}$$

where $[C]$ is the damping matrix, $[K]$ the stiffness matrix, $\{F\}$ the load vector and $\{U(t)\}$ the vector of unknowns [42]:

$$U = \{V^T, P^T, h^T\}, \tag{25}$$

for a given time step.

Equation (24) can be written as

$$\{\dot{U}\} = [C^{-1}]\{\{F\} - [K]\{U\}\} \quad \text{for} \quad t > t_0, \qquad \{U\} = \{U_0\} \quad \text{for} \quad t = t_0. \tag{26}$$

The implicit Euler method [42] is used for the transient simulation together with a Newton–Raphson procedure to solve the non-linear problem (24).

In the Euler method, Equation (26) is written at time $t + \varepsilon\Delta t$, with $0 \leq \varepsilon \leq 1$ and the time derivatives are approximated by a forward finite difference approximation:

$$\{\dot{U}_{t+\varepsilon\Delta t}\} \cong \frac{1}{\Delta t}(\{U_{t+\Delta t}\} - \{U_t\}). \tag{27}$$

The following recurrence formula is obtained:

$$\{U_{t+\Delta t}\} = \{U_t\} + \Delta t\{f(U_{t+\varepsilon\Delta t}, t + \varepsilon\Delta t)\},$$

where

$$\{U_{t+\varepsilon\Delta t}\} = \varepsilon\{U_{t+\Delta t}\} + (1-\varepsilon)\{U_t\}. \tag{28}$$

 

If $\varepsilon = 0$, the formulation corresponds to an explicit Euler method, if $0 < \varepsilon < 1$ it corresponds to the semi-implicit case, and if $\varepsilon = 1$ it corresponds to the implicit case.

The correction of $\{-\Delta U^i\}$ in $\{U_{t+\Delta t}\}$ for an iteration step $i$ of the Newton–Raphson method, is given by

$$\{-\Delta U^i_{t+\Delta t}\} = \{U^i_{t+\Delta t} - U^{i-1}_{t+\Delta t}\}, \tag{29}$$

calculated solving the system of equations

$$\left[\frac{\partial R_{nl}}{\partial U}\right]^{i-1}_{t+\Delta t} \{-\Delta U^i_{t+\Delta t}\} = \{R_{nl}\}^{i-1}_{t+\Delta t}. \tag{30}$$

The Jacobian matrix is given by

$$\left[\frac{\partial R_{nl}}{\partial U}\right]^{i-1}_{t+\Delta t} = \varepsilon\Delta t\left\{\frac{\partial F}{\partial U}\right\}^{i-1}_{t+\Delta t} - [C] - \varepsilon\Delta t\left[\frac{\partial\{K(U)\{U\}\}}{\partial U}\right]^{i-1}_{t+\Delta t}, \tag{31}$$

and the residual $\{R_{nl}\}^{i-1}_{t+\Delta t}$ is

$$\begin{aligned}\{R_{nl}\}^{i-1}_{t+\Delta t} = \Delta t(&\varepsilon\{F^{i-1}_{t+\Delta t}\} + (1-\varepsilon)\{F_t\} - (1-\varepsilon)[K(U_t)]\{U_t\} - \varepsilon[K(U^{i-1}_{t+\Delta t})]\{U^{i-1}_{t+\Delta t}\})\\ &+ [C](\{U_t\} - \{U^{i-1}_{t+\Delta t}\}).\end{aligned} \tag{32}$$

The pressure discontinuity at the interface is handled by using the double node technique [27].

The size of the time step $\Delta t$ is associated with the duration of a complete cycle of the imposed sinusoidal perturbation on feeding channel 1. The cycle time $(2\pi/\omega)$ is divided by 20 to get the integration time step $\Delta t$. Both the time step and the finite element discretization have been refined to the extent that the solutions are independent of the spatial discretization and the time interval. The degree of refinement in all finite element meshes is such that a distance of 1 mm or less has been set between nodes along the die length. The distance between nodes (and consequently between spines) is considered appropriate to capture the shape of the deforming interface for the case of the longwave instabilities studied.

The termination criteria in the Newton–Raphson procedure, for each time step, is defined by

$$\max_i|\Delta U^i_{t+\Delta t}| \le 10^{-3}, \qquad \max_i|R^i_{nl_{t+\Delta t}}| \le 10^{-3}. \tag{33}$$

The finite element mesh, for each of the geometries, has been generated using FIDAP™ [43] and then the nodal locations and interconnectivities are used for the finite element solver.

## 4. RESULTS

### *4.1. Straight channel-Newtonian fluids*

Fluid 1 (lower) with viscosity $\eta_1$, average velocity $U_1$, and depth $d_1$, and fluid 2 (upper) with viscosity $\eta_2$, average velocity $U_2$, and depth $d_2$ enter the flow domain through their corresponding feeding channels and flow downstream through the planar straight channel. The finite element mesh used for the simulations is shown in Figure 3. It consists of 424 nine-node quadrilateral elements. The channel has a length of 10 cm with 50 elements along this direction and a gap $(d = d_1 + d_2)$ of 2 cm with eight elements in this direction.

Results are compared with LSA results of Khomami [21]. Each flow system is defined in Khomami's work by its viscosity ratio $\beta$ and depth ratio $\xi$:

 

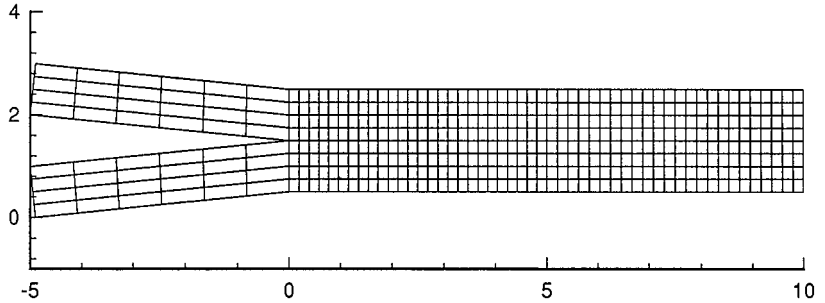


Figure 3. Finite element mesh. Straight channel die.

$$\beta = \left[\left(\frac{U_2}{d_2}\right)^{(n_1/n_2)-1}\right]\left(\frac{m_1}{m_2}\right)^{1/n_2}, \tag{34}$$

$$\xi = \frac{h}{1-h} \quad \text{where} \quad h = \frac{d_1}{d_1+d_2}. \tag{35}$$

In Equation (34) $m_1$ and $m_2$ are the consistency indices and $n_1$ and $n_2$ the power law indices of fluids 1 and 2 respectively. For the Newtonian case ($n_1 = n_2 = 1$, $m_1 = \eta_1$, $m_2 = \eta_2$), Equation (34) reduces to $\beta = \eta_1/\eta_2$.

Figure 4 depicts the interfacial instability of two Newtonian fluids as a function of the viscosity ratio ($\beta$) and the depth ratio ($\xi$) given by Khomami [21]. In Equation (35), $h$ is the dimensionless interface position ($0 < h < 1$) given by Equation (20).

The two Newtonian flow problems selected (see Figure 4) have a viscosity ratio of $\beta = 10$. The two different depth ratios ($\xi$) are obtained from a variation on the volumetric flow rate ratio ($Q_r = Q_1/Q_2$). The values of viscosity are 10 000 and 1000 Pa s respectively for fluids 1 and 2. The values of $Q_r$ are 0.125 (unstable flow) and 8 (stable flow) obtained by setting the inlet average velocity ratio ($V_{avg1}/V_{avg2}$) to the values of 0.125/1 and 1/0.125.

The simulations for the Newtonian case have been performed using a value of $\omega = 0.5$ Hz for the sinusoidal perturbation frequency imposed on feeding channel 1. With the perturbation frequency value and the steady state position and average velocity of the interface, the dimensionless wavenumber $\alpha$ is computed using Equation (23).

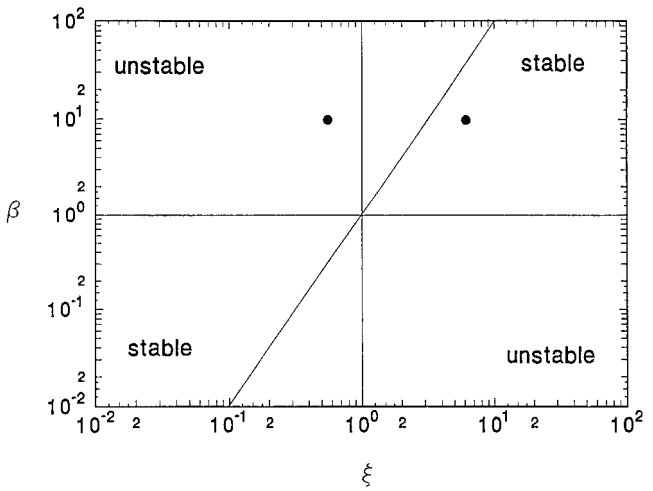


Figure 4. Interfacial stability diagram for two Newtonian fluids (Reference [21]).

 

Table II. Newtonian flow simulations (geometry shown in Figure 3)

| Parameter | Unstable Newtonian | Stable Newtonian |
|---|---|---|
| $Q_r$ | 0.125 | 8 |
| $h$ | 0.35836 | 0.86046 |
| $V_{\text{int f}}$ (cm s$^{-1}$) | 0.2979 | 0.7806 |
| $\omega$ (Hz) | 0.5 | 0.5 |
| $\alpha$ | 1.2 | 1.102 |

The time step used in the simulations was 0.6283 s, corresponding to 1/20 of a perturbation cycle time (12.566 s). The transient problem has been solved for five perturbation cycles.

Table II shows the steady state dimensionless interface position $h$, interface velocity $V_{\text{int f}}$, perturbation frequency $\omega$, and resulting dimensionless wavenumber $\alpha$ for the two Newtonian flows simulated. The results for the steady state interface position $h$ have been validated using the steady state analytical solution as a reference [44].

Figure 5(a) shows the transient behaviour of the interface for the stable Newtonian flow case. The figure corresponds to the fifth perturbation cycle. Interface shapes resulting from five different points of the perturbation cycle ($\omega t = 0$, $\pi/2$, $\pi$, $3\pi/2$, and $2\pi$) are shown. The initial steady state flat interface responds to the continuous perturbation and evolves towards the wavy pattern shown. The numerical solution shows how the amplitude of the interfacial wave decreases both in time and in the flow direction.

In order to verify that the solution was not mesh dependent or time step dependent, a second simulation was performed doubling the mesh in both directions and cutting the time step by half, and the difference between the two solutions was negligible.

Figure 5(b) shows the transient vertical movement of two points of the interface. The first is located 5 cm from the meeting point of the two fluids (center of the die), and the second one corresponds to the exit of the die (10 cm from the meeting point of the two fluids). The cyclical vertical movement of each point tends to stabilize in time. The amplitude of the wave corresponding to the exit point is lower than described by the upstream point. The stable transient solution agrees with the LSA result.

Figure 6(a) shows the Newtonian unstable flow transient movement of the interface for the fifth perturbation cycle. The amplitude of the evolving interfacial wave increases in the flow direction and is unstable, in agreement with LSA.

Figure 6(b) shows that the amplitude of the vertical movement of the downstream interfacial point (exit of the die) is larger than that described by the upstream point (center of the die), thus characterizing the flow as unstable.

### *4.2. Straight channel-Carreau fluids*

This section includes the interfacial instability study of two generalized Newtonian (Carreau model) flow systems. Two truncated power law fluids included in a linear stability analysis study by Khomami [21] are fitted using the Carreau model constitutive equation included in our model. Figure 7 shows the stability diagram for two truncated power law fluids with power law indices of $n_1 = 0.35$ and $n_2 = 0.75$, respectively [21]. The truncated power law model models a viscosity $\eta = m$ for $\dot{\gamma} \leq \dot{\gamma}_0$ and $\eta = m(\dot{\gamma}/\dot{\gamma}_0)^{n-1}$ for $\dot{\gamma} > \dot{\gamma}_0$ ($\dot{\gamma}_0 = 1$). Table III shows the rheological parameters of both fluids when fitted to the Carreau model given by Equation (8).

Table IV shows the key parameters for the two generalized Newtonian flows studied. The LSA diagram of Figure 7, given by Khomami [21], shows the location of the two flow problems in the different regions of stability.

 

Table V shows the steady state dimensionless interface position $h$, interface velocity $V_{\text{int f}}$, perturbation frequency $\omega$, and computed dimensionless wavenumber $\alpha$ for the two Carreau flow problems solved.

The time step for each simulation has been set to 1/20 of a complete perturbation cycle time, being 0.07854 s for the stable flow case and 0.7854 s for the unstable one, with five perturbation cycles accounting for the complete transient runs.

Figure 8(a) shows the developed interfacial wave corresponding to the fifth perturbation cycle of the stable flow system. It is clearly seen that the wave amplitude decreases in the flow direction. Figure 8(b) shows the transient vertical movement of the center and exit of the die interfacial points. The amplitude of the periodic movement of the downstream point is lower than that of the upstream point, thus characterizing the flow as stable.

Figure 9(a) shows the resulting interface corresponding to the fifth perturbation cycle for the case of the unstable flow system, where the interfacial wave amplitude increases in the flow

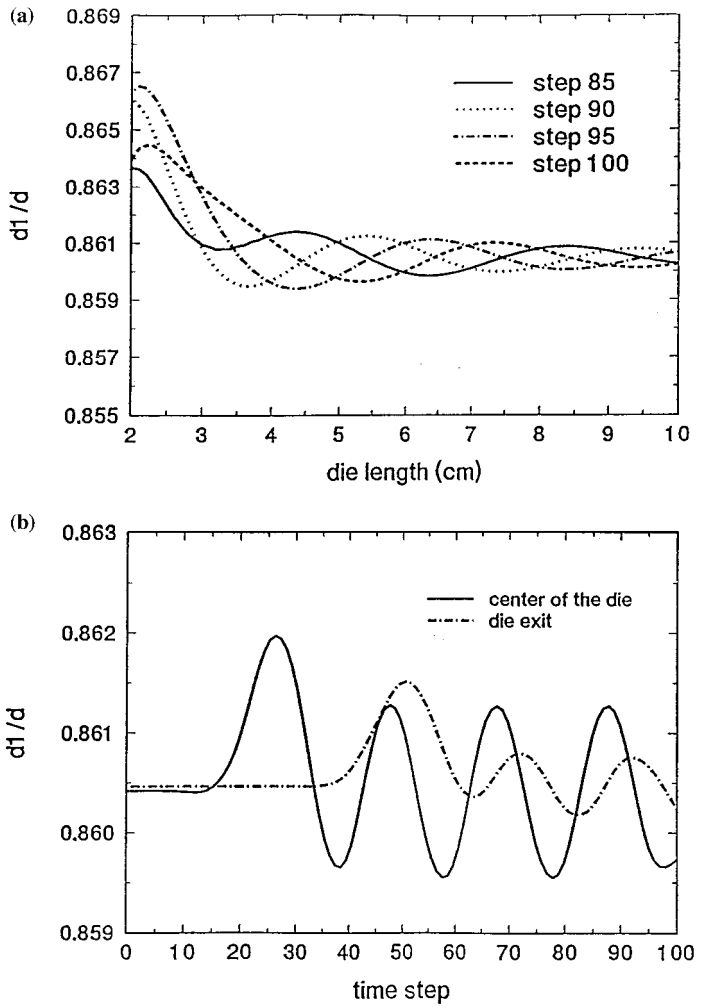


Figure 5. (a) Transient interface position. Stable Newtonian flow. $\omega = 0.5$ Hz, $\Delta t = 0.6283$ s, $\alpha = 1.102$. (b) Transient vertical movement of selected points. Stable Newtonian flow.

 

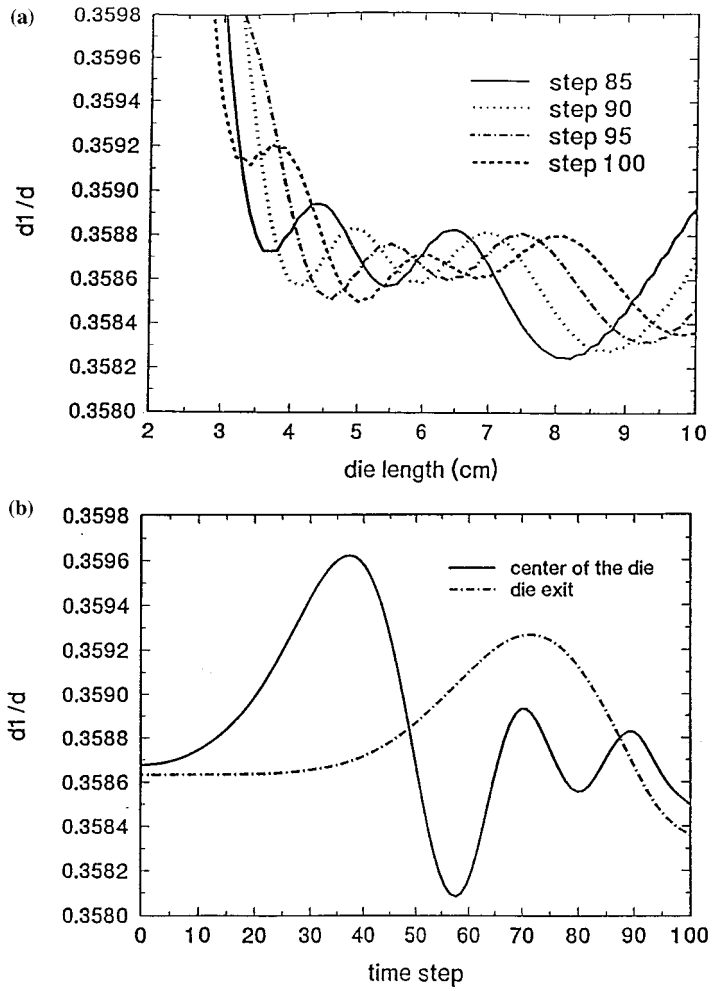


Figure 6. (a) Transient interface position. Unstable Newtonian flow. $\omega = 0.5$ Hz, $\Delta t = 0.6283$ s, $\alpha = 1.2$. (b) Transient vertical movement of selected points. Unstable Newtonian flow.

direction (Figure 9(b)). Both simulations agree with the stability prediction of the linear stability diagram of Figure 7.

### *4.3. Abrupt 2:1 expansion-Newtonian fluids*

Using the LSA theory, stability results for the two parallel plate sections of the flow channel, before and after the abrupt expansion, are compared with calculated results from the transient simulation for the entire flow field of the abrupt expansion (Figure 1(b)).

Simulations were carried out for five perturbation cycles. The perturbation frequency is 0.5 Hz. The parallel plate section of the channel before the abrupt expansion has a length of 10 cm and a gap of 2 cm (the same dimensions as the straight channel domain) and the section after the expansion has a length of 10 cm. The finite element mesh contains 100 elements in the channel length direction, with 50 elements upstream of the abrupt expansion, and 8 and 16 elements in the channel gap direction upstream and downstream of the abrupt expansion, respectively.

 

For the case of $Q_r = 8$, $\beta = 10$, $\omega = 0.5$ Hz and $\alpha = 1.102$, the steady state dimensionless interface positions $h$ for the two parallel-plate type of sections of the channel are the same with a value of 0.8575 and $\xi = 6$. Both sections of the channel are located in the stable region of the linear stability diagram of Figure 4.

Figure 10(a) shows the vertical transient movement of four selected points of the interface in the two parallel plate sections of the channel at 5 (within narrow channel), 10 (abrupt expansion), 12 (within expanded channel) and 20 cm (exit of the die) from the meeting point of the two fluids, measured in the flow direction. The figure shows the stable behaviour of the flow in the parallel plate section upstream of the abrupt expansion, with the upstream point (at 5 cm) always having a periodic movement of larger amplitude than that of the downstream point (at 10 cm). Stable flow behaviour is also observed in the parallel plate section downstream of the abrupt expansion.

For the case of $Q_r = 0.125$, $\beta = 10$, $\omega = 0.5$ Hz, $\alpha = 1.2$ and $\xi = 0.55$, both sections of the channel are in the unstable flow regime according to the linear stability diagram of Figure 4.

Figure 10(b) shows the transient vertical movement of the same interfacial points monitored at 5, 10, 12 and 20 cm along the die after the meeting point of the fluids. The amplitude of the periodic movement of the point at 10 cm becomes higher than that of the upstream point at 5 cm indicating the unstable behaviour of the flow in the upstream section of the channel. However, the downstream section of the channel shows no wavy pattern at the interface. The expansion has stabilized the flow downstream of the expansion.

### *4.4. Tapered (30°) 2:1 expansion-Newtonian fluids*

Figure 1(c) shows a schematic of the tapered expansion. The flow domain includes: an upstream parallel plate section of 10 cm in length (with 50 finite elements in this direction) and a gap of 2 cm, a tapered (30°) 2:1 expansion section of 1.732 cm (18 finite elements lengthwise) and a downstream parallel plate section of 10 cm in length (with 50 finite elements lengthwise). The number of finite elements in the cross flow direction is eight for all three sections.

For the case of $Q_r = 0.125$, $\beta = 10$, $\omega = 0.5$ Hz, $\alpha = 1.2$ and $\xi = 0.55$, results are qualitatively similar to those obtained for the abrupt expansion case, i.e. the flow is stabilized after the tapered expansion. The flow would have been unstable if the upstream parallel plate geometry had been the entire flow domain.

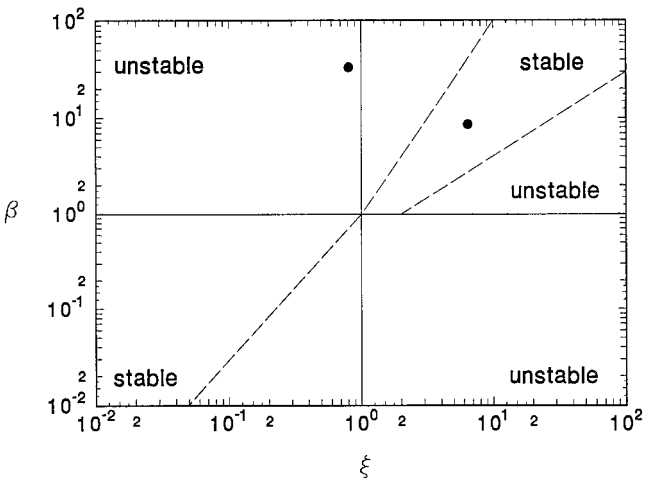


Figure 7. Interfacial stability diagram for two truncated power law fluids (Reference [21]).

 

Table III. Rheological parameters for the Carreau model

| Model parameters | Fluid 1 (lower) | Fluid 2 (upper) |
|---|---|---|
| $\lambda$ | 1.48044 | 1.68175 |
| $a$ | 2 | 2 |
| $n$ | 0.336 | 0.746 |

Table IV. Flow parameters of generalized Newtonian simulations (geometry of Figure 3)

| Parameters | Stable Carreau flow | Unstable Carreau flow |
|---|---|---|
| $U_1$ (m s$^{-1}$) | 1 | 0.0125 |
| $U_2$ (m s$^{-1}$) | 0.1 | 0.2 |
| $m_1$ (Pa s) | 7338.1 | 14 676.2 |
| $m_2$ (Pa s) | 862.7 | 862.7 |
| $\eta_{01}$ (Pa s) | 10 000 | 20 000 |
| $\eta_{02}$ (Pa s) | 1000 | 1000 |
| $\beta$ | 8.62 | 33.72 |
| $\xi$ | 6.42 | 0.81 |

Table V. Carreau fluid simulations (geometry of Figure 3)

| Parameter | Stable Carreau flow | Unstable Carreau flow |
|---|---|---|
| $h$ $(0<h<1)$ | 0.8652 | 0.3849 |
| $V_{\text{int f}}$ (cm s$^{-1}$) | 6.614 | 0.2717 |
| $\omega$ (rad s$^{-1}$) | 4 | 0.4 |
| $\alpha$ | 1.04 | 1.13 |

### *4.5. Abrupt 4:1 contraction-Newtonian fluids*

Figure 1(d) shows a schematic of the abrupt contraction. Simulations have been carried out here for different Newtonian flow systems with a fixed viscosity ratio $\beta = 10$ and volumetric flow ratio ($Q_1/Q_2$) of 1/8, 1/6, 1/5 and 8/1. All simulations include a perturbation frequency of 0.5 Hz. There are 150 elements in the channel length direction, with 100 elements in the section before the abrupt contraction (at a distance of 10 cm from the meeting point of the two fluids), and eight and four elements in the channel gap direction in the upstream and downstream sections of the channel, respectively. The depth ratio is $\xi = 6.14$ (the same in both sections of the channel) and the viscosity ratio, $\beta = 10$, which characterizes the flow as stable in both parallel plate sections of the die, according to the linear stability diagram of Figure 4. Figure 10(c) shows the vertical transient movement of four interfacial points (at 5, 10, 12, and 15 cm from the meeting point of the two fluids). The flow is stable in both sections of the contraction.

For the case where the flow is predicted to be unstable in the downstream parallel plate section for $Q_1/Q_2 = 1/8$, no possible transient solution was possible. Break-up of the interface occurred during the first time step of the transient simulation in the contraction. For the case of $Q_1/Q_2 = 1/6$, 42 complete time steps could be run before the break-up of the interface, at the abrupt contraction. This behaviour may indicate that the interface touches one of the walls so that there is no solution for which two continuous phases co-exist for the perturbation imposed. By lowering the flow rate ratio to 1/5, a complete run including five perturbation cycles could be achieved, showing a stable interface after the contraction.

 

### 4.6. Tapered (30°) 4:1 contraction-Newtonian fluids

Figure 1(e) shows a schematic of the tapered contraction. All simulations have been carried out with a perturbation frequency of 0.5 Hz. The tapered (30°) 4:1 contraction domain includes a parallel plate section upstream of the tapered contraction, of 10 cm in length and 2 cm in depth, a tapered contraction of 1.3 cm in length, and a downstream parallel plate section of 10 cm in length and 0.5 cm in depth. The finite element mesh contains 120 elements in the channel length direction, with 50 elements upstream of the abrupt expansion, 20 elements in the tapered contraction section, and 50 elements downstream of the contraction. The channel gap direction has eight elements.

For the case of $Q_1/Q_2 = 8$, the results show stable behaviour of the interface in both parallel plate sections of the die. For the case of $Q_1/Q_2 = 1/8$, 22 complete time steps can be run before the interface touches the lower wall of the tapered contraction at 10.765 cm from the meeting point of the two fluids. At $Q_1/Q_2 = 1/6$, 29 complete time steps can be run, again the interface touches the wall at 10.765 cm from the meeting point of the two fluids. With $Q_1/Q_2 = 1/5$, 38 complete time steps can be simulated with the interfacial break-up observed at 10.88 cm from the fluids meeting point (tapered contraction zone). The limiting volumetric flow rate ratio

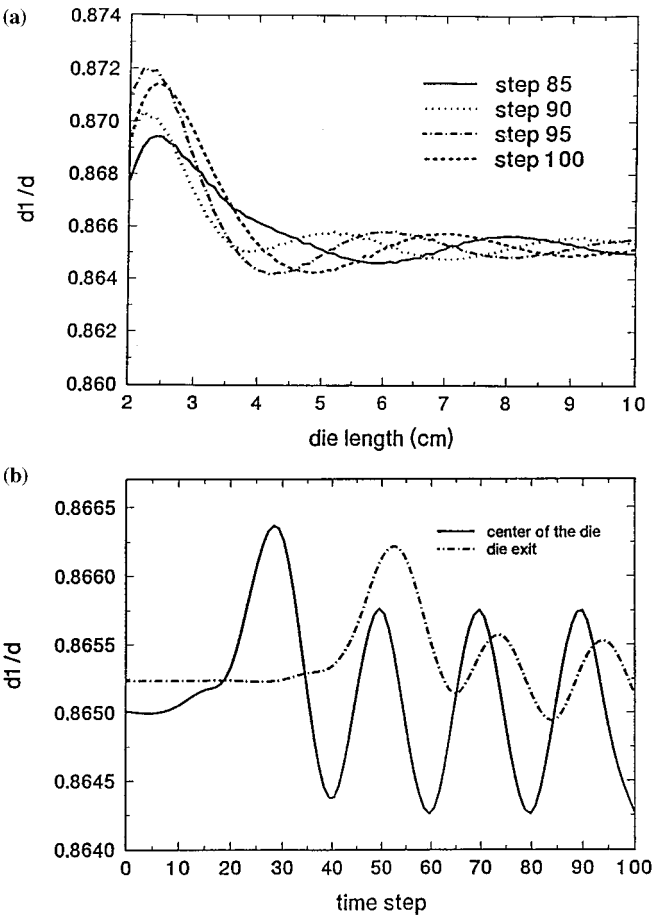


Figure 8. (a). Transient interface position. Stable Carreau model flow. $\omega = 4$ Hz, $\Delta t = 0.07854$ s, $\alpha = 1.04$. (b) Transient vertical movement of selected points. Stable Carreau model flow.

 

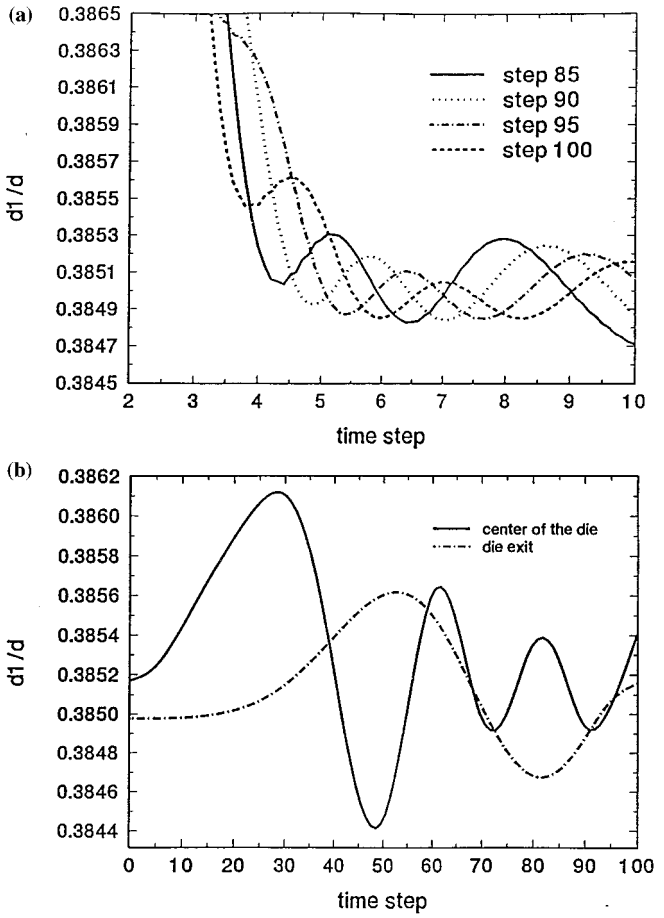


Figure 9. (a) Transient interface position. Unstable Carreau model flow. $\omega = 4$ Hz, $\Delta t = 0.7854$ s, $\alpha = 1.13$. (b) Transient vertical movement of selected points. Unstable Carreau model flow.

value before interfacial break-up has been found to be 1/4. LSA predicts unstable flow regimes for all the studied volumetric flow rate ratios ($Q_1/Q_2$).

### *4.7. Comparison against experimental work*

Simulations presented in this section correspond to the case of a parallel plate die used in the experimental work of Wilson and Khomami [7]. Figure 11 shows a schematic of the geometry which has a length of 18.542 cm and a depth of 0.254 cm. The dimensions were estimated from the available information included in the literature [7]. A qualitative comparison is made here between our simulations and the experimental results in terms of the stability of the interface.

Wilson and Khomami generated and observed interfacial instabilities in two-layer coextrusion flows by introducing temporally regular disturbances with a controllable amplitude and frequency in fluid 1. The authors developed a mechanism that forces the extruder screw forward by a predetermined amount, once each screw revolution, resulting in a pressure pulse disturbance ($P = A \sin \omega t$) with the amplitude ($A$) determined by the amount of screw displacement and the frequency ($\omega$) being identical to the screw rotation frequency. In this

 

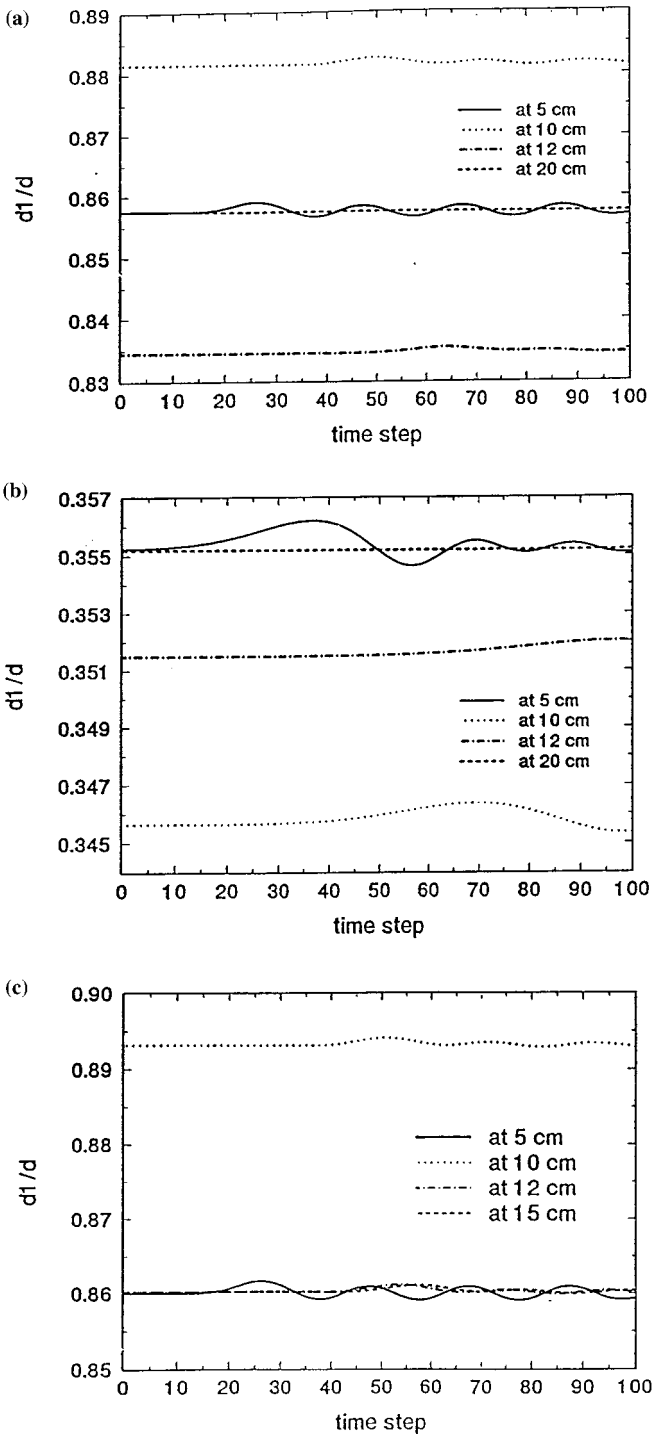


Figure 10. (a) Transient vertical movement of selected points through a 2:1 abrupt expansion. Stable Newtonian flow. $\omega = 0.5$ Hz, $\Delta t = 0.6283$ s. (b) Transient vertical movement of selected points through a 2:1 abrupt expansion. Unstable Newtonian flow. $\omega = 0.5$ Hz, $\Delta t = 0.6283$ s. (c) Transient vertical movement of selected points through a 4:1 abrupt contraction. Stable Newtonian flow. $\omega = 0.5$ Hz, $\Delta t = 0.6283$ s.

 

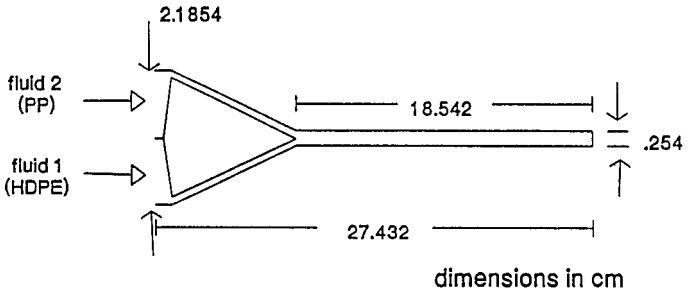


Figure 11. Geometrical domain specification of experimental die (Reference [7]).

sense, a range of dimensionless wavenumbers could be introduced, bounded by the minimum screw speed necessary to maintain the desired layer depth and by the maximum screw speed (200 rev $min^{-1}$).

In order to determine the instability or stability of a given flow, the vertical transient position of selected interfacial points are recorded into a computer and a composite image is created showing information in a temporal domain as viewed from a fixed position. This technique provides information that allows the measurement of both amplitude and frequency of the evolving interfacial wave. Thus, the growth or decay of the interfacial wave (when its amplitude is viewed at different locations along the die where viewing windows are installed) is associated with the unstable or stable behaviour of the flow respectively.

The dimensionless wavenumber ($\alpha$) given by Equation (23) is calculated here using a value of interface velocity given by the analytical solution of the flow of two polymer melts between parallel plates using a truncated power law model as the constitutive relationship. A lubrication approximation solution to the 1D equations of motion is used to calculate the interface velocity at the desired downstream position.

Two polymer systems were used in their study, a compatible system and an incompatible system. The compatible system consisted of HDPE and linear low density polyethylene (LLDPE) and the incompatible system consisted of HDPE and PP. Incompatibility implies no interaction on the molecular scale, no diffusion of one polymer species in the other and a non-zero interfacial tension.

The length scale of the interfacial waviness in the flow direction observed in the experiments was of the order of 1 cm.

The results of simulations carried out with the incompatible system (HDPE/PP) are presented. HDPE corresponds to the lower layer (fluid 1) and PP the upper layer (fluid 2). Table VI shows the fit power law coefficients, $m$ and $n$, for the given range of shear rates [7] (data for 204°C) of the HDPE and PP. Table VII contains the corresponding Carreau model rheological parameters used in the simulations. The finite element mesh has 130 elements,

Table VI. Rheological parameters for the power law model [7]

| Polymer | Type | $\gamma$ Range ($s^{-1}$) | $m$ (Pa s) | $n$ |
|---|---|---|---|---|
| Exxon PD4252 | PP | $0.1 \leq \gamma \leq 5$ | $5.08 \times 10^3$ | 0.71 |
| Quantum LS556 | HDPE | $0.1 \leq \gamma \leq 5$ | $1.17 \times 10^3$ | 0.94 |

 

Table VII. Rheological parameters for the Carreau model

| Polymer | $\mu_0$ (Pa s) | $\lambda$ | $n$ | $a$ |
|---|---|---|---|---|
| PP | 10 828.76 | 11.1576 | 0.693 | 1.8 |
| HDPE | 1314.6 | 6.41358 | 0.939 | 2 |

lengthwise, in the die section and six elements in its gap, and the amplitude of the perturbation imposed on fluid 1 is 5% of its steady state average velocity.

The first system is defined in the experimental work by a dimensionless wave number ($\alpha$) of 1 and a dimensionless interface position ($d_1/d$) of 0.2. In order to obtain the given values of $\alpha$ and $d_1/d$, the flow rate ratio ($Q_1/Q_2$) was set to 0.18 with a mean velocity of 0.018 cm $s^{-1}$ for

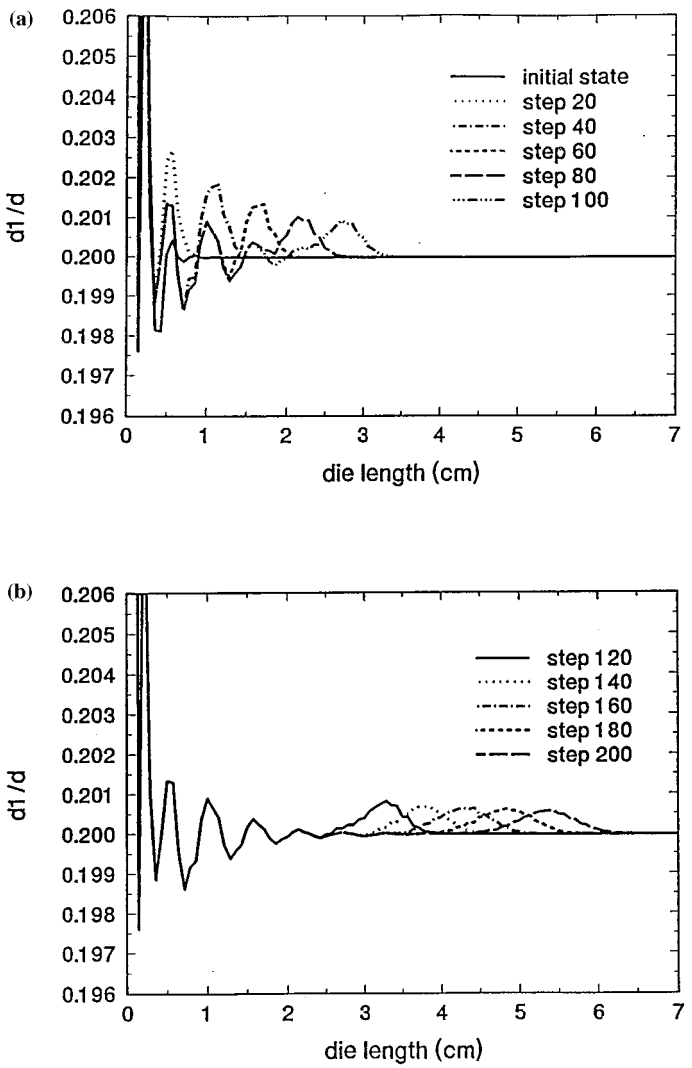


Figure 12. (a,b) Transient interface position. Stable parallel plate flow (HDPE/PP). $\omega = 3.175$ Hz, $\Delta t = 0.099$ s, $\alpha = 1$.

 

fluid 1 (HDPE) and 0.1 cm $s^{-1}$ for fluid 2 (PP). The resulting interface velocity is 0.644 cm $s^{-1}$ (calculated from a steady state solution), and the perturbation frequency is 3.17 Hz.

The complete transient simulation accounts for 200 time steps ($\Delta t = 0.099$ s). Figure 12 shows the interfacial shape monitored every 20 time steps. The transient phenomenon that takes place starts with the appearance of an interfacial waviness in the entrance of the die (Figure 12(a)). The amplitude of the interfacial wave decreases in the flow direction with the flow showing a stable behaviour. Figure 12(b) shows how the transient information travels through the die with an interfacial wave advancing towards the exit of the channel. Another key aspect observed is the shape of the interfacial wave (Figure 12(a)). The sea-wave shape type of wave is qualitatively similar to that observed experimentally. However, this asymmetry of the wave shape is observed only in the primary stages of the transient phenomenon, Figure 12(b) shows how the interfacial wave shape trends towards symmetry. The system is considered to be stable, both in simulation and experiment because the amplitude of the interface perturbation decays in the flow direction.

The second system is experimentally defined by values of $\alpha = 1$ and $d_1/d = 0.67$, and is reported as unstable. The values for $Q_1/Q_2$, interface velocity, and perturbation frequency are 3.75, 0.826 cm $s^{-1}$ and 10 Hz, respectively. Figure 13(a) and (b) show the transient interface behaviour for 300 time steps ($\Delta t = 0.0314$ s) of the simulation. The flow is experimentally unstable, but the numerical solution shows a stable flow, i.e. the amplitude of the interfacial wave decreases in the flow direction with the transient moving along the die giving rise to a second wave. This result emphasizes the need to include a viscoelastic model in the formulation to capture the stability behaviour of polymer melts.

## 5. CONCLUSIONS

The solution of the transient flow of bi-component flow systems of Newtonian and Carreau model fluids in complex geometries has been presented. By introducing a periodic perturbation in the system the transient evolution of the interface between the two fluids has been studied. Results obtained for the different parallel plate channels are in agreement with interfacial stability predictions of LSA, for both the Newtonian and the generalized Newtonian case.

Simulations of the flow in complex geometries have given new insights into the effect of flow domain geometry on the stability of a given flow system. In the case of Newtonian fluids, the inclusion of an expansion or a contraction in the channel can change the stability of the flow system. The presence of the expansion or the contraction stabilizes the flow when the flow is unstable in the section of the channel upstream of the abrupt change of geometry. For a contraction, the flow rate ratio is very important for a given contraction ratio because there are $Q_1/Q_2$ values for which no solution of continuous phases exists.

A resulting sea-wave type of wave for the case of the coextrusion flow of HDPE and PP (modeled with the Carreau equation) through a narrow gap die, indicates the combined effect of geometry and rheological parameters on the nature of the interfacial wave. However, numerical results show discrepancy with experimental findings on the coextrusion of polymer melts. The simulation of the unstable HDPE/PP flow studied shows a stable flow. This discrepancy reveals the need for a more realistic constitutive equation (viscoelastic model) to study stability phenomena in polymer melt coextrusion.

 

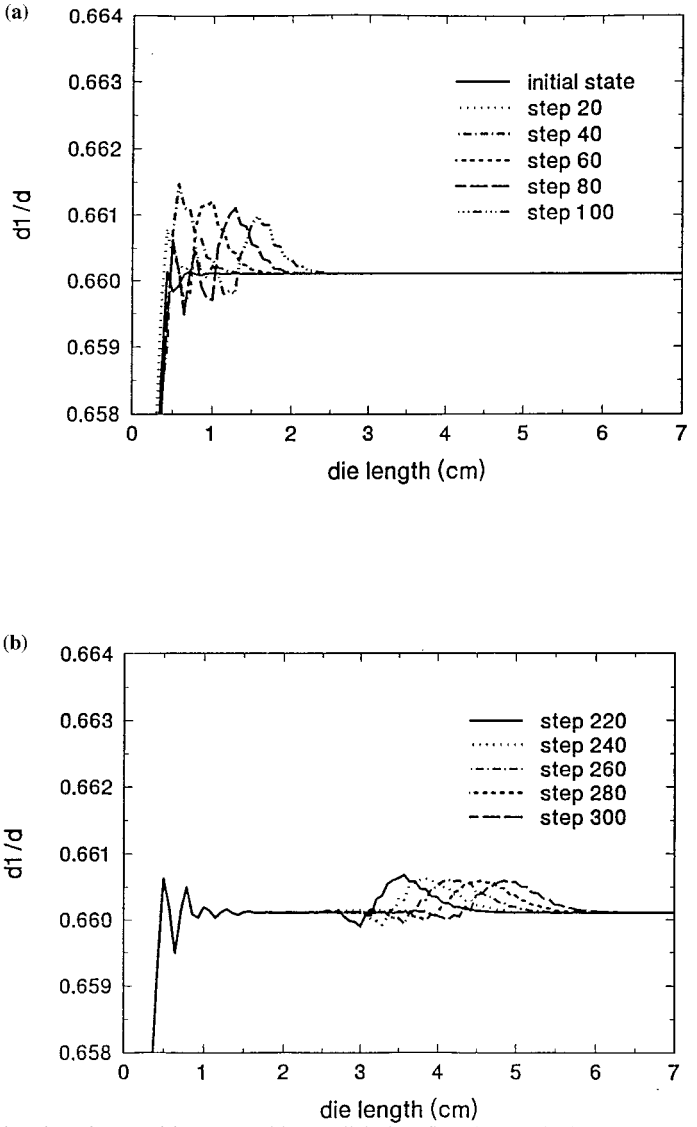


Figure 13. (a,b) Transient interface position. Unstable parallel plate flow (HDPE/PP). $\omega = 10$ Hz, $\Delta t = 0.0314$ s, $\alpha = 1$.

## ACKNOWLEDGMENTS

The authors gratefully acknowledge the financial support of the Ontario Centre for Materials Research (OCMR) and 'Investigacion y Desarrollo C.A.' (INDESCA).

## REFERENCES

1. A. Torres, A.N. Hrymak, J. Vlachopoulos, J. Dooley and B.T. Hilton, 'Boundary conditions for contact lines in coextrusion flows', *Rheol. Acta*, **32**, 513–525 (1993). Errata, *Rheol. Acta*, **33**, 241 (1994).
2. R. Ramanathan, R. Shanker, T. Rehg, S. Jons, D.L. Headley and W.J. Schrenk, 'Wave pattern instabilities in multilayer coextrusion—an experimental investigation', *SPE ANTEC*, Indianapolis, 224–228 (1996).
3. W.J. Schrenk, N.L. Bradley and T. Alfrey, 'Interfacial flow instability in multilayer coextrusion', *Polym. Eng. Sci.*, **18**, 620–623 (1978).

 

4. C.D. Han and R. Shetty, 'Studies on multilayer film coextrusion. II. Interfacial instabilities in flat film coextrusion', *Polym. Eng. Sci.*, **18**, 180–186 (1978).
5. T. Butler, 'Effects of flow instabilities in coextruded films', *Tappi J.*, **9**, 205–211 (1992).
6. H. Mavridis and R.N. Shroff, 'Multilayer extrusion: experiments and computer simulation', *Polym. Eng Sci.*, **34**, 559–569 (1994).
7. G.M. Wilson and B. Khomami, 'An experimental investigation of interfacial instabilities in multilayer flow of viscoelastic fluids. I. Incompatible polymer systems', *J. Non-Newton. Fluid Mech.*, **45**, 355–384 (1992).
8. G.M. Wilson and B. Khomami, 'An experimental investigation of interfacial instabilities in multilayer flow of viscoelastic fluids. II. Elastic and nonlinear effects in incompatible polymer systems', *J. Rheo.*, **37**, 315–339 (1993).
9. G.M. Wilson and B. Khomami, 'An experimental investigation of interfacial instabilities in multilayer flow of viscoelastic fluids. III. Compatible polymer systems', J. *Rheo.*, **37**, 340–354 (1993).
10. B. Khomami and G.M. Wilson, 'An experimental investigation of the interfacial instability in superposed flow of viscoelastic fluids in converging/diverging channel geometry', *J. Non-Newton. Fluid Mech.*, **58**, 47–65 (1995).
11. S. Hyun and M.A. Spalding, 'Use of process data obtained from a data acquisition system for optimizing and debugging extrusion processes', *Adv. Polym. Tech.*, **15**, 29–40 (1996).
12. Z. Tadmor and I. Klein, *Engineering Principles of Plasticating Extrusion*, Van Nostrand Reinhold, New York, 1970.
13. C.S. Yih, 'Instability due to viscosity stratification', *J. Fluid Mech.*, **27**, 337–352 (1967).
14. C.E. Hickox, 'Instability due to viscosity stratification in axisymmetric pipe flow', *Phys. Fluids*, **14**, 251–262 (1971).
15. C.H. Li, 'Stability of two superposed elastoviscous liquids in plane Couette flow', *Phys. Fluids*, **12**, 531–538 (1969).
16. A.A. Khan and C.D. Han, 'A study on the interfacial instability in the stratified flow of two viscoelastic fluids through a rectangular duct', *Trans. Soc. Rheol.*, **21**, 101–131 (1977).
17. K.P. Chen, 'Elastic instability on the interface in Couette flow of viscoelastic liquids', *J. Non-Newton. Fluid Mech.*, **40**, 261–267 (1991).
18. A.P. Hooper and W.G. Boyd, 'Shear-flow instability at the interface between two viscous fluids', *J. Fluid Mech.*, **128**, 507–528 (1983).
19. D.D. Joseph, M. Renardy and Y. Renardy, 'Instability of the flow of two immiscible liquids with different viscosities in a pipe', *J. Fluid Mech.*, **141**, 309–317 (1984).
20. N.D. Waters, 'The stability of two stratified power-law fluids in Couette flow', *J. Non-Newton. Fluid Mech.*, **12**, 85–94 (1983).
21. B. Khomami, 'Interfacial instability and deformation of two stratified power law fluids in plane Poiseuille flow', *J. Non-Newton. Fluid Mech.*, **36**, 289–303 (1990).
22. B. Khomami, 'Interfacial stability and deformation of two stratified power law fluids in plane Poiseuille flow. 2. Interface deformation', *J. Non-Newton. Fluid Mech.*, **37**, 19–36 (1990).
23. Y.Y. Su and B. Khomami, 'Interfacial instability of multilayer viscoelastic fluids in slit and converging channel die geometries', *J. Rheo.*, **36**, 357–387 (1992).
24. Y.Y. Su and B. Khomami, 'Stability of multilayer power law and second order fluids in Poiseuille flow', *Chem. Eng. Commun.*, **109**, 209–223 (1992).
25. Y.Y. Su and B. Khomami, 'Purely elastic interfacial instabilities in superposed flow of polymeric fluids', *Rheol. Acta*, **31**, 413–420 (1992).
26. E. Mitsoulis, 'Extrudate swell in double layer flows', *J. Rheo.*, **30(S)**, S23–S44 (1986).
27. H. Mavridis, A.N. Hrymak and J. Vlachopoulos, 'Finite-element simulation of stratified multiphase flows', *AIChE J.*, **33**, 410–422 (1987).
28. A. Karagiannis, H. Mavridis, A.N. Hrymak and J. Vlachopoulos, 'Interface determination in bicomponent extrusion', *Polym. Eng. Sci.*, **28**, 982–988 (1988).
29. E. Mitsoulis and F.L. Heng, 'Numerical simulation of coextrusion from a circular die', *J. Appl. Polym. Sci.*, **34**, 1713–1725 (1987).
30. J. Dheur and M.J. Crochet, 'Newtonian stratified flow through an abrupt expansion', *Rheol. Acta*, **26**, 401–413 (1987).
31. D.M. Binding, K. Walters, J. Dheur and M.J. Crochet, 'Interfacial effects in the flow of viscous and elastoviscous liquids', *Phil. Trans. R. Soc. Lond.*, **A323**, 424–469 (1987).
32. S. Musarra and R. Keunings, 'Co-current axisymmetric flow in complex geometries: Numerical simulation', *J. Non-Newton. Fluid Mech.*, **32**, 253–268, (1989).
33. R. Ramanathan and J. Dooley, 'Dynamics of multilayer polymer melt flow: An experimental and numerical investigation', *SPEANTEC*, Detroit, 426–430 (1992).
34. D.R. Lynch, 'Unified approach to simulation on deforming elements with application to phase change problems', *J. Comput. Phys.*, **47**, 387–411 (1982).
35. H.S. Kheshgi and L.E. Scriven, 'Penalty-finite element analysis of time-dependent two dimensional free surface film flows', in T Kawai (ed.), *Finite Elements in Fluids*, Wiley, New York, 1984, pp. 113–120.
36. P.M. Gresho, R.L. Lee and R.L. Sani, 'On the time dependent solution of the incompressible Navier–Stokes equations in two and three dimensions', in *Recent Advances in Numerical Methods in Fluids*, Vol. 1, Pineridge Press, Swansea, UK, 1979.

 

37. S.F. Kistler and L.E. Scriven, 'Coating flow theory by finite element and asysmptotic analysis of the Navier–Stokes system', *Int. J. Numer. Methods Fluids*, **4**, 207–229 (1984).
38. R. Keunings, 'An algorithm for the simulation of transient viscoelastic flow with free surfaces', *J. Comput. Phys.*, **62**, 199–220 (1986).
39. B. Ramaswamy, 'Numerical simulation of unsteady viscous free surface flow', *J. Comput. Phys.*, **90**, 396–430 (1990).
40. N.R. Anturkar, 'Mechanics and stability of multilayer extrusion', *Ph.D. Thesis*, The University of Michigan, 1990.
41. R.B. Bird, W.E. Stewart and E.N. Lightfoot, *Transport Phenomena*, Wiley, New York, 1960.
42. G. Dhatt and G. Touzot, *The Finite Element Method Displayed*, Wiley, New York, 1984.
43. *FIDAP (Fluid Dynamics Analysis Package)*, *Version 7.0*, *Theory Manual*, 1993.
44. C.D. Han, *Multiphase Flow in Polymer Processing*, Academic Press, New York, 1981.

 